ATTRIBUTION OF A RECORD-BREAKING HEATWAVE EVENT IN SUMMER 2017 OVER THE YANGTZE RIVER DELTA

Chunlüe Zhou, Kaicun Wang, Dan Qi, and Jianguo Tan

The occurrence probability of the record-breaking Yangtze River Delta heatwave in summer 2017 might be attributed to global warming (23%), the abnormal western Pacific subtropical high (32%), and the urban heat island effect (58%).

INTRODUCTION. During 11 to 28 July 2017, the Yangtze River Delta experienced a record-breaking heatwave. In particular, the Xujiahui weather station in Shanghai endured the worst heatwave in at least 145 years, with a new record of 40.9°C on 21 July 2017. The extreme heatwave left four people dead and many elderly people and children suffering from heatstroke.

Generally, the western Pacific subtropical high (WPSH) is regarded as the key anticyclone system for the occurrence of extreme heatwave events in eastern China (Yang and Li 2005; Ding et al. 2010; Wang et al. 2014; Luo and Lau 2017; Wang et al. 2016; Li and Sun 2018). The WPSH variability is modulated by tropical forcing from sea surface temperature anomalies over the equatorial Pacific Ocean (e.g., ENSO) (Tao and Xu 1962; Wang et al. 2000; He et al. 2015a; Chen and Zhou 2017) and over the tropical Indian Ocean (Yang et al. 2007; Du et al. 2009; Xie et al. 2009). During the decaying El Niño, the lasting warming over the tropical Indian Ocean can trigger an anomalous WPSH by exciting Kelvin waves eastward (Wu et al. 2009; Wu et al. 2010), resulting in a westward extension of the WPSH (Huang and Wu 1989; Zhou et al. 2009). The west-extending WPSH induces an anomalous southwesterly flow to transport more moisture to the northern regions and then dry the atmosphere over the Yangtze River Delta (Chen and Lu 2015). This process results in decreased rainfall and increased surface incident solar radiance (Hu et al. 2012, 2013; Liu et al. 2015; Chen et al. 2016; Freychet et al. 2017), which introduce extreme heatwaves in the Yangtze River Delta, such as the one in 2013 (Li et al. 2015).

Other known factors that increase the risk of heatwaves over the Yangtze River Delta include anthropogenic global warming (Yang and Li 2005; Sun et al. 2014; Zhou et al. 2014), which meanwhile influences the variations of the WPSH by tropical oceanic warming (Zhou et al. 2009; He and Zhou 2015; He et al. 2015b), and the urban heat island effect due to local urbanization around the weather stations, which can exacerbate the heatwave by enhancing sensible heat flux and longwave radiation from the surface during the daytime (Tan et al. 2008; Sun et al. 2016; J. Wang et al. 2017).

Using the heatwave magnitude index (HWMI) and July–August mean temperature to quantify the 2017 heatwave, this study therefore tries to answer two questions: 1) How extreme is the heatwave over the Yangtze River Delta in a historical context? 2) What are the relative impacts of the WPSH, global warming, and the urban heat island on the heatwave?

DATA AND METHODS. Daily maximum air temperature (T_{max}) from 1961 to 2017 at ~2400 meteorological stations (Fig. 1) are collected (available at http://data.cma.cn/). Data from 1873 to 2017 at the Xujiahui station are used to depict century-long temperature change (Tan et al. 2008). Following Russo et al. (2014), this study defines the HWMI by considering the duration and intensity of a heatwave, that is, the maximum magnitude of the heatwaves in summer (June–September), where a heatwave has at

AFFILIATIONS: Zhou and Wang—College of Global Change and Earth System Science, Beijing Normal University, Beijing, China; Qi—National Meteorological Center, China Meteorological Administration, Beijing, China; Tan—Key Laboratory of Cities Mitigation and Adaptation to Climate Change in Shanghai, Shanghai Climate Center, Shanghai, China
CORRESPONDING AUTHOR: Kaicun Wang, kcwang@bnu.edu.cn

DOI:10.1175/BAMS-D-18-0134.1

A supplement to this article is available online (10.1175/BAMS-D-18-0134.2)

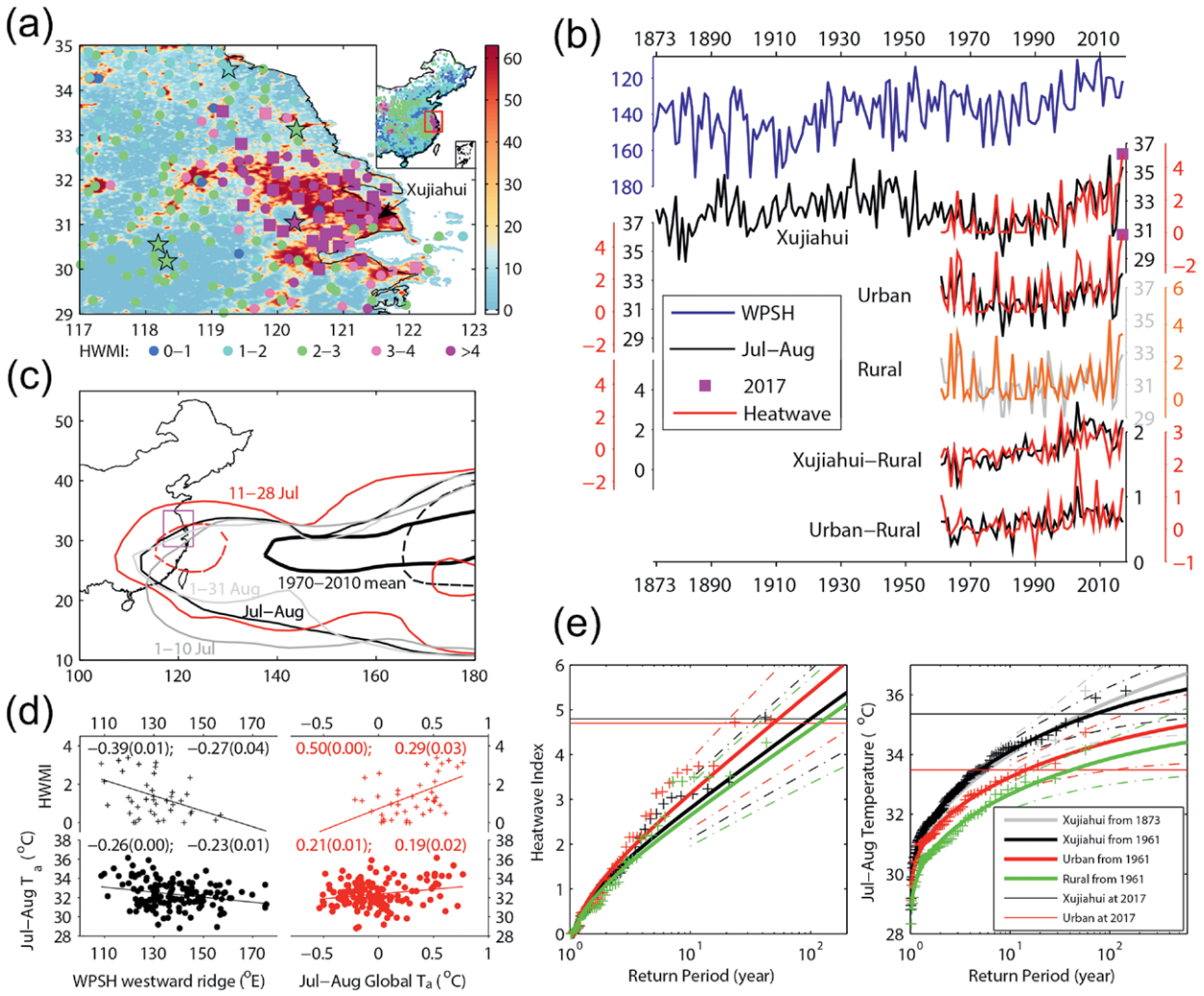

Fig. 1. (a) Spatial pattern of observed extreme heat (denoted by the HWMI) in summer of 2017 over the Yangtze River Delta, China. The stations having the record-breaking heatwave in 2017 during the period of 1961–2017 are plotted in squares. The HWMI categories are as folows: ≤1 normal <2 ≤ moderate <3 ≤ severe <4 ≤ extreme. Stable lights from the defense meteorological satellite program are used to describe metropolis and rural regions. (b) Time series of the July–August mean west-extending ridge point position of the western Pacific subtropical high (WPSH) (in blue lines), and the July–August means of daily maximum air temperatures (in black lines) and the HWMI (in red lines) over Xujiahui station (from 1873), for urban and rural regions. Temperature differences between at Xujiahui station in the downtown area or urban stations at the edge of urban area and rural stations imply the urban heat island effect on maximum air temperature change. (c) Changes in the 588-dagpm contours before and after the 2017 heatwave in 11–28 July. During these days, the 588-dagpm contour centers in the Yangtze River Delta, intensifying the heatwave. (d) The July–August mean temperature and the HWMI show significant correlations with the July–August mean west-extending ridge point position of WPSH and global mean temperature anomalies with $p < 0.01$ before detrending (numbers in left column of each subfigure) and $p < 0.04$ after detrending the time series (numbers in right columns). (e) GEV fit (in solid lines) of the July–August mean temperature and the HWMI with 95% confidence intervals (in dashed lines).

least three consecutive days with T_{max} exceeding the 90th percentile (centered on a 30-day window) for the reference period of 1971–2000 (Fischer and Schär 2010). We find that 80% of the maximum heatwaves happen in July and August (see Fig. ES1 in the online supplemental material).

Following the procedure of Ren et al. (2015), five rural stations (shown by stars in Fig. 1a) are identified in comparison with urban stations to quantify the urban heat island effect. The west-extending ridge point position (WRPP) index of the WPSH is calculated (Tao and Xu 1962; Ding 1994; Liu et al. 2012) with the

2.5° × 2.5° 500-hPa geopotential height of the NOAA-CIRES Twentieth Century Reanalysis from 1873 to 2014 (Compo et al. 2011) and extended to 2017 by that of National Centers for Environmental Prediction Reanalysis (NCEP-R1) (Kalnay et al. 1996; Zhou et al. 2018a). We define the years with a WRPP index smaller (larger) than the climatological value (e.g., 137.5°E in reanalysis) as strong (weak) WPSH years. Note that the WRPP index has a near-linear relationship with the area index of the WPSH (Fig. ES1). The WRPP index can be also estimated by use of CMIP5 experiments (Zhou and Li 2002; Dong et al. 2017). After evaluations of the all-forcings (ALL) simulations in CMIP5 archive (Taylor et al. 2012), 19 simulations in seven models (Table ES1 and Fig. ES2) with T_{max} extended through 2017 (Sun et al. 2014) and having corresponding natural-forcings-only simulations (NAT) ending in 2012 are selected to estimate the influence of anthropogenic global warming. These detailed procedures can be found in the online supplemental information.

For consistency with the observational analysis, the model data are area-averaged over the study region (117°–123°E, 29°–35°N) (Fig. 1a). We apply several statistical techniques to assess the heatwave over the Yangtze River Delta:

1) A Kolmogorov–Smirnoff test (K-S) is conducted to determine how well the distributions of the simulated temperature anomalies match the observed distribution.
2) Generalized extreme value (GEV) (Schaller et al. 2016) and scaled GEV (van der Wiel et al. 2017; Zhou et al. 2018b) distributions are determined to fit the observed and modeled HWMI and July–August temperature (see the online supplemental information).
3) The probability ratio (PR = P_{urban}/P_{rural}) is calculated to quantify urban heat island effect in the odds of extreme heat. The terms P_{urban} and P_{rural} represent the probabilities exceeding a threshold of the 2017 extreme event in two different observation scenarios (i.e., urban and rural regions). After excluding the urban heat island effect, the fraction of attributable risk (FAR = $1 - P_{NAT}/P_{ALL}$ or $1 - P_{weakWPSH}/P_{strongWPSH}$) method (Stone and Allen 2005) is used to separate the influences of global warming and the WPSH through several combinations of simulation scenarios even though it is difficult to accurately quantify their influences. We estimate the influence of global warming by setting P_{ALL} to be the probability exceeding the 2017 extreme event under the strong WPSH in ALL simulations, with P_{NAT} being the equivalent for the NAT simulations. Accordingly, we compare the probabilities of the 2017 extreme event under strong and weak WPSHs (i.e., $P_{strongWPSH}$ and $P_{weakWPSH}$) in ALL simulations for estimating the WPSH influence. The 95% confidence intervals (CI) are estimated with a 1000-member bootstrap (with replacement).

RESULTS. *Influence of the urban heat island.* Figure 1a illustrates the spatial pattern of the 2017 extreme heatwave over the Yangtze River Delta. The record-breaking heatwave in 2017 mainly occurred in the Shanghai metropolitan area (in squares of Fig. 1a), particularly with up to 4.84 HWMI in Xujiahui station and 4.77 HWMI in the urban region (Fig. 1b). The Xujiahui station is located downtown in a built-up area with high population density (Fig. 1a), which in turn leads to higher temperatures recorded than at other stations that are located at the edge of the urban region. A GEV fit of the observed HWMI denotes that the 2017 extreme heat is a 1-in-53-yr event for in the urban region and 1-in-104-yr event for Xujiahui station (Fig. 1e). However, the HWMI in the rural region was not the maximum in 2017 (a 1-in-28-yr event; Fig. 1e), but it was in 2013 (Fig. 1b).

Temperature differences between urban and rural stations are suggested to reflect urbanization-induced warming (Sun et al. 2016). Urbanization-induced warming of the HWMI is 0.30°C decade^{-1} (significance level p = 0.00, accounting for 70% of the HWMI warming trend) at Xujiahui station and 0.11°C decade^{-1} (p = 0.00; 48%) in the urban region (Fig. 1b). For 2017, the values are 38% and 36%, respectively (Fig. 1b).

July–August temperature in 2017 is a 1-in-70-yr event in Xujiahui station and a 1-in-15-yr event for the urban region, which is not extreme in a historical context (Figs. 1b,e). Urbanization-induced July–August temperature warming is 0.35°C decade^{-1} (p = 0.00; 84%) at Xujiahui station and 0.05°C decade^{-1} (p = 0.00; 64%) in the urban region (Fig. 1b). For 2017, the values are 83% and 2% (calculated as the percentage of urbanization-induced temperature anomaly to temperature anomaly in 2017), respectively (Fig. 1b). More (less) partitioning of surface incident solar radiation into sensible (latent) heat flux induced by impervious surfaces in the urban region can largely explain the urbanization-induced warming in summer over the Yangtze River Delta (Wang and Dickinson 2013; Zhou and Wang 2016; K. Wang et al. 2017).

In addition, from the view of event occurrence probability, the urban heat island increases the likelihood of the 2017 extreme heat over the Yangtze River Delta by 2.5 times [(95% CI: 1.9–4.1) for the

HWMI; cf. 3.0 times (95% CI: 2.4–4.0) for July–August temperature] (Figs. 1e and 2c). In other words, 58% [(95% CI: 47%–76%) for the HWMI; cf. 67% (95% CI: 58%–75%) for July–August temperature] of the attributable risk of the heatwave is caused by the urban heat island.

Influence of the WPSH. The HWMI and July–August temperature anomalies show evident decadal variations (Fig. 1b), which are revealed to correlate with the WPSH ($r = -0.39$ and -0.26, $p < 0.01$, respectively) (Fig. 1d). The 588 dagpm (1 dagpm = 10 geopotential meters) of WPSH was located at ~25°N in early July (1–10 July 2017), and moved northward as well as extended westward to the Yangtze River Delta in middle to late July (11–28 July 2017), bringing the anomalous anticyclone over this region and favoring local heating by increasing surface incident solar radiation (Fig. 1c). After the heatwave, the WPSH retreated to ~27°N in August (Fig. 1c).

Compared with the likelihood of the HWMI between strong and weak WPSH in the ALL simulations,

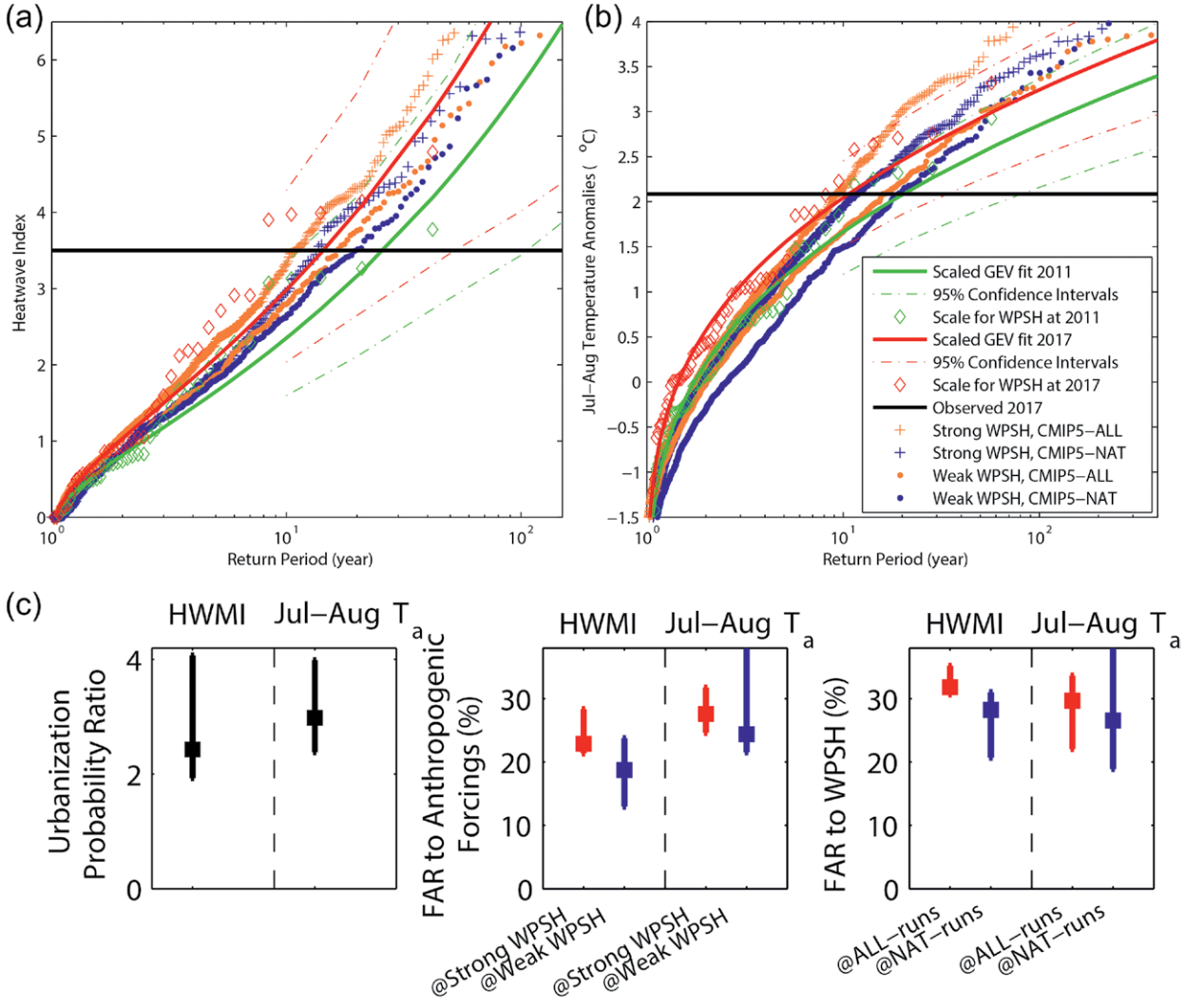

Fig. 2. (a) Return period (unit: yr) of the HWMI from the observations and models participating in phase 5 of the Coupled Model Intercomparison Project (CMIP5) under different conditions, including all forcings (ALL) and natural forcing only (NAT) simulations. The brown/blue crosses (circles) indicate strong (weak) WPSH years from the ALL and NAT simulations. The dashed lines are the 95% confidence intervals of the scaled generalized extreme value (GEV) fit to the climate in 2011 and 2017, respectively. The black thick line is the observed average HWMI of 2017 at rural regions. (b) As in (a), but for the July–August mean temperature. (c) Probability ratio (PR; %) of the HWMI and the July–August mean temperature due to urbanization and the fraction of attributable risk (FAR; %) to anthropogenic forcings and the WPSH are calculated under two different runs including the ALL and NAT simulations. Best estimates and corresponding 95% confidence intervals are calculated by the 1000-member nonparametric bootstrap.

we find 32% [(95% CI: 31%–35%) for the HWMI; cf. 30% (95% CI: 22%–33%) for July–August temperature] of the attributable risk of the 2017 extreme heatwave is attributed to the WPSH. In NAT simulations, the FAR is slightly smaller, 28% [95% CI: 20%–31% for the HWMI; cf. 26% (95% CI: 23%–94%) for July–August temperature] (Fig. 2).

Influence of anthropogenic global warming. The HWMI and July–August temperature anomalies have significantly positive correlations with July–August global mean air temperature (r = 0.50 and 0.21, $p < 0.01$, respectively) (Fig. 1d), implying the footprint of global warming on the 2017 extreme heat.

To assess the influence of global warming, we compare the changes in the likelihood of the HWMI from the ALL and NAT runs (Fig. 2a). Given the strong WPSH, 23% [95% CI: 21%–28% for the HWMI; cf. 27% (95% CI: 25%–32%) for July–August temperature] of the attributable risk of such events as the 2017 extreme heatwave is attributed to global warming (Fig. 2). Given the weak WPSH, the FAR is slightly smaller (i.e., 18%) [95% CI: 11%–24% for the HWMI; cf. 24% (95% CI: 21%–92%) for July–August temperature, calculated from the return periods of approximately 15 and 20 years in ALL and NAT runs] (Fig. 2).

CONCLUSIONS AND DISCUSSION. Our analysis based on the HWMI indicates that the record-breaking heatwave event of 2017 is a 1-in-104-yr event at the Xujiahui station and a 1-in-58-yr event over the Yangtze River Delta. CMIP5-based FAR analyses suggest that approximately 23% (95% CI: 21%–28%) of the risk of such events might be attributed to global warming and 32% (95% CI: 31%–35%) of the risk might be due to the WPSH. The urban heat island over the metropolis increases the likelihood of such events by 2.5 times and contributes 36% of severity of the 2017 extreme heatwave over the Yangtze River Delta. In a word, the westward extension of the WPSH likely leads to the formation of the extreme heatwave, and global warming as well as the urban heat island would further increase the severity of the heatwave.

Zhou et al. (2014) pointed out but did not disentangle the role of global warming and internal climate variability in the 2013 extreme heat over middle and lower reaches of the Yangtze River. Zhou et al. (2014) reported 58% of attributable risk to global warming, which is near the sum (27% + 30% = 57%) of attributable risk to global warming and the WPSH in the 2017 extreme heat over the Yangtze River Delta.

We find that the FAR of such events over the Yangtze River Delta to the WPSH is relatively higher than that to global warming. In a strong WPSH (often leading to the extreme heat), global warming will have a slightly larger role in increasing the likelihood of such events as the 2017 extreme heat than that in a weak WPSH. In ALL simulations (often leading to the extreme heat), the role of the WPSH is also slightly higher than that in NAT runs. These results above further imply that both global warming and the WPSH will increase the likelihood of such events as the 2017 extreme heat over the Yangtze River Delta.

ACKNOWLEDGMENTS. This study was funded by the National Key R&D Program of China (2017YFA0603601) and the National Natural Science Foundation of China (41525018). Dan Qi was supported by the National Natural Science Foundation of China (41475044). The latest temperature data were obtained from the China Meteorological Administration (CMA; http://data.cma.cn/). Considerable gratitude is owed to several working teams, including the National Oceanic and Atmospheric Agency (NOAA) and the University of Colorado's Cooperative Institute for Research in Environmental Sciences (CIRES) for providing the atmospheric fields (www.esrl.noaa.gov/), the National Geophysical Data Centers of NOAA for providing stable nighttime light data (http://ngdc.noaa.gov/eog/dmsp), the World Climate Research Programme's Working Group on Coupled Modelling (http://cmip-pcmdi.llnl.gov/cmip5/), and the Royal Netherlands Meteorological Institute (https://climexp.knmi.nl/) for the CMIP5 model output. Chunlüe Zhou dedicates this in loving memory of his kind father and his heartwarming encouragement forever.

REFERENCES

Chen, R., and R. Lu, 2015: Comparisons of the circulation anomalies associated with extreme heat in different regions of eastern China. *J. Climate*, **28**, 5830–5844, https://doi.org/10.1175/JCLI-D-14-00818.1.

——, Z. Wen, and R. Lu, 2016: Evolution of the circulation anomalies and the quasi-biweekly oscillations associated with extreme heat events in southern China. *J. Climate*, **29**, 6909–6921, https://doi.org/10.1175/JCLI-D-16-0160.1.

Chen, X., and T. Zhou, 2017: Relative contributions of external SST forcing and internal atmospheric variability to July–August heat waves over the Yangtze River valley. *Climate Dyn.*, https://doi.org/10.1007/s00382-017-3871-y.

Compo, G. P., and Coauthors, 2011: The Twentieth Century Reanalysis Project. *Quart. J. Roy. Meteor. Soc.*, **137**, 1–28, https://doi.org/10.1002/qj.776.

Ding, T., W. Qian, and Z. Yan, 2010: Changes in hot days and heat waves in China during 1961–2007. *Int. J. Climatol.*, **30**, 1452–1462, https://doi.org/10.1002/joc.1989.

Ding, Y., 1994: The summer monsoon in East Asia. *Monsoons over China*, Springer, 1–90.

Dong, X., F. Fan, R. Lin, J. Jin, and R. Lian, 2017: Simulation of the western North Pacific subtropical high in El Niño decaying summers by CMIP5 AGCMs. *Atmos. Oceanic Sci. Lett.*, **10**, 146-155, https://doi.org/10.1080/16742834.2017.1272404.

Du, Y., S.-P. Xie, G. Huang, and K. Hu, 2009: Role of air–sea interaction in the long persistence of El Niño–induced north Indian Ocean warming. *J. Climate*, **22**, 2023–2038, https://doi.org/10.1175/2008JCLI2590.1.

Fischer, E., and C. Schär, 2010: Consistent geographical patterns of changes in high-impact European heatwaves. *Nat. Geosci.*, **3**, 398–403, https://doi.org/10.1038/ngeo866.

Freychet, N., S. Tett, J. Wang, and G. Hegerl, 2017: Summer heat waves over eastern China: Dynamical processes and trend attribution. *Environ. Res. Lett.*, **12**, 024015, https://doi.org/10.1088/1748-9326/aa5ba3.

He, C., and T. Zhou, 2015: Responses of the western North Pacific subtropical high to global warming under RCP4.5 and RCP8.5 scenarios projected by 33 CMIP5 models: The dominance of tropical Indian Ocean–tropical western Pacific SST gradient. *J. Climate*, **28**, 365–380, https://doi.org/10.1175/JCLI-D-13-00494.1.

——, ——, and B. Wu, 2015a: The key oceanic regions responsible for the interannual variability of the western North Pacific subtropical high and associated mechanisms. *J. Meteor. Res.*, **29**, 562–575, https://doi.org/10.1007/s13351-015-5037-3.

——, ——, A. Lin, B. Wu, D. Gu, C. Li, and B. Zheng, 2015b: Enhanced or weakened western North Pacific subtropical high under global warming? *Sci. Rep.*, **5**, 16771, https://doi.org/10.1038/srep16771.

Hu, K., G. Huang, X. Qu, and R. Huang, 2012: The impact of Indian Ocean variability on high temperature extremes across the southern Yangtze River valley in late summer. *Adv. Atmos. Sci.*, **29**, 91–100, https://doi.org/10.1007/s00376-011-0209-2.

——, ——, and R. Wu, 2013: A strengthened influence of ENSO on August high temperature extremes over the southern Yangtze River valley since the late 1980s. *J. Climate*, **26**, 2205–2221, https://doi.org/10.1175/JCLI-D-12-00277.1.

Huang, R., and Y. Wu, 1989: The influence of ENSO on the summer climate change in China and its mechanism. *Adv. Atmos. Sci.*, **6**, 21–32, https://doi.org/10.1007/BF02656915.

Kalnay, E., and Coauthors, 1996: The NCEP/NCAR 40-Year Reanalysis Project. *Bull. Amer. Meteor. Soc.*, **77**, 437–471, https://doi.org/10.1175/1520-0477(1996)077<0437:TNYRP>2.0.CO;2.

Li, J., T. Ding, X. Jia, and X. Zhao, 2015: Analysis on the extreme heat wave over China around Yangtze River region in the summer of 2013 and its main contributing factors. *Adv. Meteor.*, **2015**, 706713, https://doi.org/10.1155/2015/706713.

Li, R.-X., and J.-Q. Sun, 2018: Interdecadal variability of the large-scale extreme hot event frequency over the middle and lower reaches of the Yangtze River basin and its related atmospheric patterns. *Atmos. Ocean. Sci. Lett.*, **11**, 63–70, https://doi.org/10.1080/16742834.2017.1335580.

Liu, G., R. Wu, S. Sun, and H. Wang, 2015: Synergistic contribution of precipitation anomalies over northwestern India and the South China Sea to high temperature over the Yangtze River Valley. *Adv. Atmos. Sci.*, **32**, 1255–1265, https://doi.org/10.1007/s00376-015-4280-y.

Liu, Y., W. Li, W. Ai, and Q. Li, 2012: Reconstruction and application of the monthly western Pacific subtropical high indices. *J. Appl. Meteor. Sci.*, **23**, 414–423.

Luo, M., and N.-C. Lau, 2017: Heat waves in southern China: Synoptic behavior, long-term change and urbanization effects. *J. Climate*, **30**, 703–720, https://doi.org/10.1175/JCLI-D-16-0269.1.

Ren, G., and Coauthors, 2015: An integrated procedure to determine a reference station network for evaluating and adjusting urban bias in surface air temperature data. *J. Appl. Meteor. Climatol.*, **54**, 1248–1266, https://doi.org/10.1175/JAMC-D-14-0295.1.

Russo, S., and Coauthors, 2014: Magnitude of extreme heat waves in present climate and their projection in a warming world. *J. Geophys. Res.*, **119**, 12 500–12 512, https://doi.org/10.1002/2014JD022098.

Schaller, N., and Coauthors, 2016: Human influence on climate in the 2014 southern England winter floods and their impacts. *Nat. Climate Change*, **6**, 627–634, https://doi.org/10.1038/nclimate2927.

Stone, D. A., and M. R. Allen, 2005: The end-to-end attribution problem: From emissions to impacts. *Climatic Change*, **71**, 303–318, https://doi.org/10.1007/s10584-005-6778-2.

Sun, Y., X. Zhang, F. W. Zwiers, L. Song, H. Wan, T. Hu, H. Yin, and G. Ren, 2014: Rapid increase in the risk of extreme summer heat in eastern China. *Nat. Climate Change*, **4**, 1082–1085, https://doi.org/10.1038/nclimate2410.

——, ——, G. Ren, F. W. Zwiers, and T. Hu, 2016: Contribution of urbanization to warming in China. *Nat. Climate Change*, **6**, 706–710, https://doi.org/10.1038/nclimate2956.

Tan, J., Y. Zheng, L. Peng, S. Gu, and J. Shi, 2008: Effect of urban heat island on heat waves in summer of Shanghai. *Plateau Meteor.*, **27**, 144–149.

Tao, S., and S. Xu, 1962: Circulation characteristics in association with persistent summer drought and flood in the Yangtze-Huaihe River reaches. *Acta Meteor. Sin.*, **32**, 1–18.

Taylor, K. E., R. J. Stouffer, and G. A. Meehl, 2012: An overview of CMIP5 and the experiment design. *Bull. Amer. Meteor. Soc.*, **93**, 485–498, https://doi.org/10.1175/BAMS-D-11-00094.1.

van der Wiel, K., and Coauthors, 2017: Rapid attribution of the August 2016 flood-inducing extreme precipitation in south Louisiana to climate change. *Hydrol. Earth Syst. Sci.*, **21**, 897–921, https://doi.org/10.5194/hess-21-897-2017.

Wang, B., R. Wu, and X. Fu, 2000: Pacific–East Asian teleconnection: How does ENSO affect East Asian climate? *J. Climate*, **13**, 1517–1536, https://doi.org/10.1175/1520-0442(2000)013<1517:PEATHD>2.0.CO;2.

Wang, J., Z. Yan, X.-W. Quan, and J. Feng, 2017: Urban warming in the 2013 summer heat wave in eastern China. *Climate Dyn.*, **48**, 3015–3033, https://doi.org/10.1007/s00382-016-3248-7.

Wang, K., and R. E. Dickinson, 2013: Contribution of solar radiation to decadal temperature variability over land. *Proc. Natl. Acad. Sci. USA*, **110**, 14 877–14 882, https://doi.org/10.1073/pnas.1311433110.

——, S. Jiang, J. Wang, C. Zhou, X. Wang, and X. Lee, 2017: Comparing the diurnal and seasonal variabilities of atmospheric and surface urban heat islands based on the Beijing urban meteorological network. *J. Geophys. Res.*, **122**, 2131–2154, https://doi.org/10.1002/2016JD025304.

Wang, W., W. Zhou, and D. Chen, 2014: Summer high temperature extremes in southeast China: Bonding with the El Niño–Southern Oscillation and East Asian summer monsoon coupled system. *J. Climate*, **27**, 4122–4138, https://doi.org/10.1175/JCLI-D-13-00545.1.

——, ——, X. Li, X. Wang, and D. Wang, 2016: Synoptic-scale characteristics and atmospheric controls of summer heat waves in China. *Climate Dyn.*, **46**, 2923–2941, https://doi.org/10.1007/s00382-015-2741-8.

Wu, B., T. Zhou, and T. Li, 2009: Seasonally evolving dominant interannual variability modes of East Asian climate. *J. Climate*, **22**, 2992–3005, https://doi.org/10.1175/2008JCLI2710.1.

——, T. Li, and T. Zhou, 2010: Relative contributions of the Indian Ocean and local SST anomalies to the maintenance of the western North Pacific anomalous anticyclone during the El Niño decaying summer. *J. Climate*, **23**, 2974–2986, https://doi.org/10.1175/2010JCLI3300.1.

Xie, S.-P., K. Hu, J. Hafner, H. Tokinaga, Y. Du, G. Huang, and T. Sampe, 2009: Indian Ocean capacitor effect on Indo–western Pacific climate during the summer following El Niño. *J. Climate*, **22**, 730–747, https://doi.org/10.1175/2008JCLI2544.1.

Yang, H., and C. Li, 2005: Diagnostic study of serious high temperature over south China in 2003 summer. *Climate Environ. Res.*, **10**, 80–85.

Yang, J., Q. Liu, S. P. Xie, Z. Liu, and L. Wu, 2007: Impact of the Indian Ocean SST basin mode on the Asian summer monsoon. *Geophys. Res. Lett.*, **34**, L02708, https://doi.org/10.1029/2006GL028571.

Zhou, C., and K. Wang, 2016: Biological and environmental controls on evaporative fractions at AmeriFlux sites. *J. Appl. Meteor. Climatol.*, **55**, 145–161, https://doi.org/10.1175/JAMC-D-15-0126.1.

——, Y. He, and K. Wang, 2018a: On the suitability of current atmospheric reanalyses for regional warming studies over China. *Atmos. Chem. Phys.*, **18**, 8113–8136, https://doi.org/10.5194/acp-18-8113-2018.

——, K. Wang, and D. Qi, 2018b: Attribution of the July 2016 extreme precipitation event over China's Wuhang [in "Explaining Extreme Events of 2016 from a Climate Perspective"]. *Bull. Amer. Meteor. Soc.*, **99**, S107–S112, https://doi.org/10.1175/BAMS-D-17-0090.1.

Zhou, T., and Z. Li, 2002: Simulation of the East Asian summer monsoon using a variable resolution atmospheric GCM. *Climate Dyn.*, **19**, 167–180, https://doi.org/10.1007/s00382-001-0214-8.

——, and Coauthors, 2009: Why the western Pacific subtropical high has extended westward since the late 1970s. *J. Climate*, **22**, 2199–2215, https://doi.org/10.1175/2008JCLI2527.1.

——, S. Ma, and L. Zou, 2014: Understanding a hot summer in central eastern China: Summer 2013 in context of multimodel trend analysis [in "Explaining Extreme Events of 2013 from a Climate Perspective"]. *Bull. Amer. Meteor. Soc.*, **95**, S54–S57, https://doi.org/10.1175/1520-0477-95.9.S1.1.